Journal of Medicinal Chemistry

Article

Identifying Novel Selective Non-Nucleoside DNA Methyltransferase 1 Inhibitors through Docking-Based Virtual Screening

Shijie Chen, Yulan Wang, Wen Zhou, Shanshan Li, Jianlong Peng, Zhe Shi, Junchi Hu, Yu-Chih Liu, Hong Ding, Yijyun Lin, Linjuan Li, Sufang Cheng, Jingqiu Liu, Tao Lu, Hualiang Jiang, Bo Liu, Mingyue Zheng, and Cheng Luo

J. Med. Chem., **Just Accepted Manuscript** • DOI: 10.1021/jm501134e • Publication Date (Web): 21 Oct 2014

Identifying Novel Selective Non-Nucleoside DNA Methyltransferase 1 Inhibitors through Docking-Based Virtual Screening

Shijie Chen[#,¶], Yulan Wang[#,¶], Wen Zhou[II,¶], Shanshan Li[‡], Jianlong Peng[#], Zhe Shi[|], Junchi Hu[#], Yu-Chih Liu[|], Hong Ding[#], Yijyun Lin[|], Linjuan Li[#,§], Sufang Cheng[#], Jingqiu Liu[#], Tao Lu[‡], Hualiang Jiang[#,§], Bo Liu[II,*], Mingyue Zheng[#,*] and Cheng Luo[#,*]

[#]State Key Laboratory of Drug Research, Shanghai Institute of Materia Medica, Chinese Academy of Sciences, 555 Zuchongzhi Road, Shanghai 201203, China

[‡]Laboratory of Molecular Design and Drug Discovery, School of Science, China Pharmaceutical University, 24 Tongjiaxiang, Nanjing 210009, China

[|]In Vitro Biology, Shanghai ChemPartner LifeScience Co., Ltd., #5 Building,998 Halei Road, Shanghai 201203, China

[II]Guangdong Provincial Academy of Chinese Medical Sciences (The Second Affiliated Hospital of Guangzhou University of Chinese Medicine), 55 Neihuanxi Road, Guangzhou 510006, China

[§]School of Life Science and Technology, Shanghai Tech University, Shanghai 200031, China

[¶]These authors contributed equally to this work.

*Correspondence:

Bo Liu: Telphone, 86-20-39318571. Email: doctliu@263.net.

Mingyue Zheng : Telphone, 86-21-50806600. Email: myzheng@simm.ac.cn.

Cheng Luo: Telphone, 86-20-50806600. Email: cluo@simm.ac.cn.

Abstract

The DNA methyltransferases (DNMTs) found in mammals include DNMT1, DNMT3A and DNMT3B, and are attractive targets in cancer chemotherapy. DNMT1 was the first among the DNMTs to be characterized, and it is responsible for maintaining DNA methylation patterns. A number of DNMT inhibitors have been reported, but most of them are nucleoside analogs that can lead to toxic side-effects and lack specificity. By combining docking-based virtual screening with biochemical analyses, we identified a novel compound, DC_05. DC_05 is a non-nucleoside DNMT1 inhibitor with low micromolar IC_{50} values and significant selectivity towards other AdoMet-dependent protein methyltransferases. Through a process of similarity-based analog searching, compounds DC_501 and DC_517 were found to be more potent than DC_05. These three potent compounds significantly inhibited cancer cell proliferation. The structure-activity relationship (SAR) and binding modes of these inhibitors were also analyzed to assist in the future development of more potent and more specific DNMT1 inhibitors.

Introduction

Epigenetic modifications such as DNA methylation, histone methylation and histone acetylation play essential roles in all aspects of biology.[1] Among all the epigenetic events, DNA methylation is most likely the best-known epigenetic marker and has been shown to participate in gene expression control.[2] In mammals, DNA methylation occurs at the 5-position of cytosine, almost as in the context of CpG dinucleotides that are clustered in CpG islands.[1, 3] In cancer cells, alterations in DNA methylation can lead to promoter hypermethylation at CpG islands and then silence tumor suppressor genes.[4] Unlike genetic origins, aberrations in DNA methylation are reversible, thus allowing cancer cells to revert to their normal state.[5] To date, DNMT1, DNMT3A and DNMT3B are the three different DNA methyltransferases that have been identified in mammals.[6, 7] DNMT1 is the most abundant among the three, and it serves as a substrate for hemimethylated CpG dinucleotides and is responsible for maintaining DNA methylation patterns in mammals.[6, 8] DNMT3A and DNMT3B are associated with de novo methylation during embryonic development.[9] The inhibition of DNA methyltransferase activity can reactivate silenced tumor suppressor genes (TSGs),[10] and thus, DNMT inhibitors have become useful tools to revert cancer cells.

Two types of DNMT inhibitors have been discovered, namely nucleoside analogs and non-nucleoside analogs.[1] Two nucleoside analogs, 5-azacytidine (Vidaza) and 5-aza-2'-deoxycytidine (Decitabine), have been approved by the FDA for treating myelodysplastic syndrome and leukemia.[2] However, these drugs can reportedly be incorporated into DNA and cause covalent trapping and the subsequent depletion of DNMTs.[11] Moreover, these drugs are unstable, show low specificity and have significant toxic side-effects.[12] Specific interest has therefore been generated in non-nucleosides. As shown in Chart 1, various non-nucleoside analogs have been reported, including the following: natural compounds such as genistein,[13] (-)-epigallocatechin-3-O-gallate (EGCG),[14] and laccaic acid A;[15] repurposed drugs such as hydralazine (hypertension antagonist),[16] procainamide and procaine (antiarrhythmic and anesthetic agents, respectively);[17, 18] novel inhibitors such as phthalimido-L-tryptophan (RG108);[4, 19] and the quinolone

derivative SGI-1027.[20] In comparison with nucleoside analogs, non-nucleoside analogs are less likely to be incorporated into DNA and hence offer a safer way to target DNA methylation. Unfortunately, the potency of known non-nucleoside DNMT inhibitors is much lower than that of nucleoside analogs, and most of DNMT inhibitors are multi-target inhibitors with unknown mechanisms of action.[12, 21] Moreover, as shown in Chart 1, the demethylating activities of natural compounds and redirected drugs remain controversial.[22, 23] There are two reported non-nucleoside DNMT inhibitors called SGI-1027 (IC_{50} = 35 ± 3 μM)[24] and RG108 (IC_{50} = 390 ± 50 μM)[25] that may cause demethylation by inhibiting DNMT directly, and their detailed mechanisms of action remain unknown.[19, 20] At present, there are no non-nucleoside DNMT inhibitors entering clinical trials, and it is therefore highly important to develop new DNMT inhibitors.

The virtual screening of compound databases has emerged as a powerful computational approach, and it is also increasingly used in drug discovery projects.[26-30] In addition to its convenience and low cost, this technique can also help identify novel scaffolds, understand the binding mode of the active compound, and provide some indications for compound optimization. In addition, virtual screening can also be complemented with other ligand-based approaches, such as similarity searching. To date, several successful docking-based virtual screenings have been conducted with DNMT1.[4, 31, 32]

In this study, docking-based virtual screening was used to search for novel DNMT1 inhibitors from the SPECS database. Highly ranked compounds were subjected to cluster analysis through virtual screening by Glide. Fifty-one compounds were selected and purchased for further DNMT1 inhibitor bioactivity testing. Because it had a high inhibition rate, DC_05 was also the most potent compound in the group and showed remarkable selectivity toward DNMT1. We therefore used this compound to obtain more structural analogs within the SPECS database, and 19 analogs were selected to perform the bioactivity assay. DC_501 and DC_517 both exhibited increased inhibitory potency in the enzymatic assays. Further experimental studies demonstrated that these three potent compounds significantly inhibited cancer cell proliferation. Taken together, this study indicates that DC_05 and its analogs are new potential DNMT1 inhibitors, and they can

provide us with new structural clues to develop more potent DNMT1 inhibitors.

Results and discussion

Docking-Based Virtual Screening. In the present study, a docking-based virtual screening strategy was used to identify promising hits. The crystal structure of mouse DNMT1 bound to *S*-adenosyl-L-homocysteine (SAH) and cytosine (PDB entry: 4DA4)[33] was used for molecular docking. This structure was selected because it is present in an active form and contains both the cofactor and DNA substrate. The protein structure was prepared in the Protein Preparation Wizard Workflow of the Schrödinger software package. The SPECS database (heep://www.specs.net) containing 198,745 compounds was used as a ligand database. First, the compounds with unfavorable physicochemical properties were filtered out using Pipeline Pilot 7.5. After removing the compounds with unfavorable properties, the remaining 111,121 compounds were prepared with LigPrep to generate all stereoisomers and different protonation states by Epik. The prepared ligands were docked in the SAH and cytosine-binding pocket of DNMT1 protein with the Glide module in Schrödinger. The docking procedure was validated by reproducing the SAH binding mode with a root-mean-square deviation (RMSD) of 0.6 Å (Figure S1 in supporting information (SI)). According to the Glide scores (GScores) and structural clustering, 51 structurally diverse compounds were selected and purchased for biochemical assay. The structures and docking scores of the 51 compounds are provided in Table S1 in the SI.

DNMT1 Inhibition Assays. The 51 candidate molecules selected by virtual screening were tested for DNMT1 inhibition to validate their biochemical activities. From the ELISA DNMT1 activity assay, we used the EpiQuik DNA Methyltransferase (DNMT) Activity/Inhibitor Assay Kit (Epigentek) and identified DC_05 for its ability to inhibit DNMT1 activity by >60%, and this compound had a similar potency to that of SAH against DNMT1 at a concentration of 200 μM. In a more quantitative analysis, we measured the methyltransferase activity of DNMT1 at a range of concentrations for this compound using the H-3-labeled

radioactive methylation assay and the IC_{50} value derived from the dose response curve, which was 10.3 μM (Figure 1). We also performed agarose gel electrophoresis to identify whether DC_05 binds to DNA.[34] Doxorubicin was used as a positive control, and it has been shown to interact with DNA[35]. SGI-1027 was reported to bind slightly to DNA[20], and it was also used as a positive control. SAH was used as a negative control. As shown in Figure S2, doxorubicin and SGI-1027 change the migration rate of DNA at higher concentrations, and the decrease in emission intensity could be considered the result of EB (DNA bound) replacement. By contrast, DC_05 and DC_517 have no such effect on the DNA and show similar results to the negative SAH control and the DNA control without inhibitors. These results suggest that our compounds do not act by binding to DNA. All the results suggest that DC_05 could be characterized as a structurally novel DNMT1 inhibitor with a remarkable potency against DNMT1.

The Methyltransferase Enzymatic Selectivity of DC_05. In addition to DNMT1, there are many other methyltransferases that can bind with *S*-adenosyl-L-methionine (SAM) to facilitate transmethylation reactions. To investigate the selectivity of DC_05 for DNMT1, the compound was also evaluated for its inhibitory activities against other important methyltransferases, including DNMT3A, DNMT3B and other AdoMet-dependent enzymes, such as G9a (histone H3 lysine 9 methyltransferase),[36] SUV39H1 (histone H3 lysine 9 methyltransferase),[37] MLL1 (histone H3 lysine 4 methyltransferase),[38, 39] SET7/9 (histone H3 lysine 4 methyltransferase)[40] and PRMT1 (arginine methyltransferase).[41] Under the tested conditions, DC_05 inhibited PRMT1 at a potency that was 3.6-fold weaker than that of DNMT1. Moreover, it showed nearly no inhibitory activities against DNMT3A, DNMT3B, MLL1, SET7/9, SUV39H1 and G9a (Table 1, Figure S3). All these findings demonstrated that DC_05 is a DNMT1-selective inhibitor. Here, the selectivity of non-nucleoside DNMT1 inhibitors is somewhat expected because these methyltransferases catalyze different substrates and share a very low homology with DNMT1, even in their catalytic domain. The low conservation of structure is revealed from the multiple sequence alignment analysis provided in Figure S4, and among these comparisons, DNMT3A/3B and PRMT1 show relatively higher sequence identities with

DNMT1. To understand the basis of this selectivity, we superimposed the catalytic sites of DNMT1, DNMT3A and PRMT1, and we briefly discuss the potential reasons for DC_05 selectivity in the supporting information (Figure S5).

Similarity-Based Analog Searching and a Radioactive Methylation Assay Against DNMT1. In accordance with the general notion that similar compounds have similar activity levels, similarity-based analog searching was conducted to select the compounds of interest. Because compound DC_05 has a relatively high IC_{50} activity and good selectivity, an analog search using DC_05 as the query template was performed to select more potential hit compounds. Finally, 19 compounds with similar scaffolds were purchased from SPECS Corp, and their inhibitory activities against DNMT1 were assessed. Although most of those compounds have chirality centers, the purchased samples were in the racemic form. Table 2 shows the generic chemical structures of these compounds and their inhibitory activities against DNMT1. The inhibition potencies are expressed as the inhibition rates at a concentration of 50 μM. As shown both in Table 2 and Figure 2, 8 of the 19 compounds showed more than 50% inhibition of the DNMT1 activity at 50 μM. We then tested these potent compounds within a range of concentrations by radioactive methylation assay to compare with DC_05. DC_501 (IC_{50} = 2.5 μM) and DC_517 (IC_{50} = 1.7 μM) displayed 4.1- and 6.0-fold higher activity than DC_05 against DNMT1, and DC_503, DC_504, DC_508, DC_514 and DC_516 analogs were less potent, respectively. DC_512 showed a similar inhibitory activity as DC_05 (Table 2, Figure S6). This second round of compound searching and screening helped us to find many more potential compounds that inhibited DNMT1 activity, and the results uncovered important information for hit optimization and the study of structure-activity relationships (SARs).

Surface Plasmon Resonance (SPR)-based Binding Assay. To more precisely validate these potential DNMT1 inhibitors, we used the SPR-based binding assay to measure direct interactions between DNMT1 and the compounds. As shown in Figure 3, the interactions were dose dependent and strong, further confirming the activity of these potential compounds. The equilibrium dissociation constant (K_D) between

DC_05 and DNMT1 is approximately 1.09 μM, and that of DC_517 is 0.91 μM. In comparison with compound DC_05, DC_517 showed a higher affinity for DNMT1, which was consistent with the DNMT1 inhibition potency levels. However, because of the limited characterization of compound DC_501, we did not obtain good SPR curves to calculate the K_D between DC_501 and DNMT1.

Analyzing Chiral Enantiomers of DC_05 and DC_517. As shown in Table 2, DC_05 and its analogs contain chiral centers, and the samples we purchased from SPECS are in racemic mixtures. DC_05 and DC_517 enantiomers were synthesized to understand the effect of chirality on the activities of these compounds. Radioactive methylation assays were performed to determine the activities of the DC_05 and DC_517 enantiomers, in addition to their racemates. As shown in Figure 4B, (*R*)-DC_05 (IC_{50} = 7.3 μM) and (*S*)-DC_05 (IC_{50} = 15.6 μM) show slightly different activities towards DNMT1, and the (*R*)- and (*S*)-enantiomers of DC_517 show very similar potencies (Figure 4E).

Molecular docking studies were also performed, and the putative binding modes of both enantiomers within DNMT1 were carefully inspected (Figure 4C, F). The binding poses of (*R*)-DC_05 and (*S*)-DC_05 with DNMT1 closely resemble one another (Figure 4C). Both the carbazolyls of (*R*)-DC_05 and (*S*)-DC_05 are located in a large hydrophobic pocket formed by F1148, C1194, D1193 and M1172 in the SAM pocket and establish a cation–π interaction with K1247, and the indolyls occupy the cytosine pocket and make hydrogen bonds through the amino to E1269. Despite these similarities, their hydroxyls form hydrogen bonds with different residues, in which the hydrogen bond in (*R*)-DC_05 involves the E1171 residue, and it involves the K1247 residue in (*S*)-DC_05 (Figure 4C). E1171 is a conserved residue at the SAM pocket of DNMTs and forms a hydrogen bond with SAH, but K1247 does not. The slightly different activities of (*R*)- and (*S*)-DC_05 may therefore be caused by the different hydrogen bonds with different residues. To account for the improved inhibitory potency and the chiral effect of DC_517, we analyzed their interactions with DNMT1. As shown in Figure 4F, one carbazolyl of DC_517 is located in the hydrophobic pocket of the SAM pocket, which resembles DC_05 binding, and the other carbazolyl stretches outside the SAM pocket

and interacts with R1576, which has been shown to be an important residue that forms interactions with DNMT1 inhibitors.[3, 24, 25] Because R1576 is less than 4 Å away and has a carbazolyl group outside the SAM pocket, the improved potency observed in DC_517 can therefore be ascribed to the gain of a cation-π interaction with R1576. In addition, the hydroxyl group of DC_517 forms hydrogen bonds with E1171, and the imino group interacts with the primary chain oxygen of F1148. In comparing the putative binding poses of two DC_517 enantiomers, we may find that they closely match with one another, which is consistent with their activity assay results. The 2D ligand interaction diagrams of DC_05 and DC_517 enantiomers are provided in Figures S7 and S8. In general, the binding modes of the enantiomers of these two compounds within DNMT1 only show subtle differences that are consistent with their biochemical activities. These results suggested that the chirality of the reported compound series may play a less important role in determining their binding and activity toward DNMT1.

SAR Analysis. The structure-activity relationship of DC_05 and its analogs were identified and investigated by similarity searching. As shown in Table 2, we found that the compounds with either scaffolds I or II contain carbazolyl, and the compounds with scaffolds III and VI do not. Their DNMT1 inhibitory activities suggest that the carbazolyl is essential for their activity. The putative binding poses of the compounds in Table 2 were analyzed to understand the molecular basis for DNMT1 inhibition using the carbazolyl molecule series. As shown in Figure 5A, the catalytic site of DNMT1 can be divided into two parts, namely the cofactor binding site SAM pocket and the substrate binding site cytosine pocket, which are depicted as a dashed green circle and a dashed orange circle, respectively. The carbazolyl groups of DC_05 is located in the SAM pocket and establishes a cation–π interaction with K1247, and the indolyl group is located in the cytosine pocket and forms a hydrogen bond via its imino group to E1269. To study the effects of the substituents on the aliphatic chain (R1 and R3 in Table 2) in this activity, we compared the binding poses of DC_05, DC_503, DC_504, DC_508 and DC_516. Figure 5B shows that they share a similar pattern, and it shows that their filling of the cytosine pocket varies (Figure 5B). Generally, a better occupation of the

cytosine pocket corresponds to a higher inhibitory activity, and this result is consistent with a study by Asgatay *et al*.[25] For DC_05, the hydrogen bond formed with E1269 is essential to its binding because E1269 also forms a hydrogen bond with the cytosine and mediates the catalytic reaction under physiological conditions.[33, 42] In the SAM pocket, the carbazolyl of (*R*)- and (*S*)-DC_05 are located in a large hydrophobic region, and their hydroxyl groups form hydrogen bonds with E1171 and K1247, respectively (Figure 4C). Similar interactions were also observed for the compounds displayed in Figure 5B, which suggests that the hydrogen bonds are helpful for anchoring the carbazolyl group directly to the SAM pocket. The imino groups (pKb≈3.1) of DC_05 and its analogs should mostly exist as a protonated aminium form at the given pH (pH = 7.0±2.0), which was set by preparing ligand structures. There were ionic interactions between these amino ions and E1171, which are barely affected by compound chirality. As mentioned above, most hydroxyl groups in the compounds could form hydrogen bonds with E1171 or K1247, regardless of which chirality they have. These interactions may explain why the chiral center does not have a major influence on the binding affinity. Moreover, the chlorine (Cl) and bromine (Br) on the carbazolyl appear to be beneficial to the inhibitory activity of these compounds because DC_501 (Figure 5C) is more potent than DC_05, and DC_512 (Figure 5D) is more potent than DC_504 and DC_508. Because the halogen substituents on the aromatic ring are typical hydrophobicity-enhancing groups, the increased activities of DC_501 and DC_512 can be partially ascribed to the reinforced hydrophobic interactions with the large hydrophobic region of the SAM binding site. In addition, the lone pairs of the halogen substituents may also stabilize the cation–π interaction of the carbazolyl with K1247. Another notable point is that DC_512 does not occupy the cytosine pocket in comparison with DC_501, but the extra hydrogen bond formed with G1226 stabilizes its binding, and the DC_512 activity is maintained (IC_{50} = 14.1 μM). To understand the improved potency of DC_512, we compared the 2D ligand interaction diagrams of DC_512 with those of DC_504 and DC_508 and give a brief discussion in Figure S9. As analyzed above, the improved potency of compound DC_517 can be attributed to the cation-π interaction between its outward carbazolyl and R1576, which has been highlighted

as an important residue that interacts with other non-nucleoside DNMT inhibitors.[3, 24, 25] However, from a ligand efficiency (LE) perspective, DC_517 (LE = 0.21) is slightly inferior to DC_05 (LE = 0.24), which suggests that the increased hydrophobic and cation-π interactions are weak intermolecular forces and only lead to a less significant gain in affinity. To achieve a more effective interaction with R1576, the carbazolyl of DC_517 should be replaced by smaller groups, such as phenyl or other small negatively charged groups.

Cell-Based Activity. Collectively, compounds DC_05, DC_501 and DC_517 showed potential DNMT1-inhibiting activity in vitro, and we further explored whether these three most intriguing compounds would affect the proliferation of cancer cells. We tested DC_05, DC_501 and DC_517 in HCT116 (human colon cancer) and Capan-1 (human pancreatic adenocarcinoma cells). An MTT assay was performed to determine the compounds' effects on cell proliferation and viability. In regular culture medium, DC_05, DC_501 and DC_517 significantly inhibited cell proliferation at a low concentration. The dose- and time-dependent inhibition profiles shown in Figure 6 clearly indicate that these compounds have remarkable activities both *in vitro* and *ex vivo* (Figure 6A, B). As mentioned above, the enantiomers of DC_05 show slightly different activities toward DNMT1, and the (*R*) and (*S*) enantiomers of DC_517 show very close potencies *in vitro*. To understand the effect of the chirality on the proliferation of HCT116 and Capan-1 cells, we tested DC_05, (*R*)-DC_05, (*S*)-DC_05, DC_517, (*R*)-DC_517 and (*S*)-DC_517 on these two cell types. Figure S10 shows that the enantiomers display the same level of anti-proliferative activities as their corresponding racemates, which are also consistent with their DNMT1 inhibition potencies as determined by radioactive methylation assay.

Notably, DC_517 displayed the highest anti-proliferative effects in the two types of cancer cells, and this result was also fully consistent with the biochemical assay results. Moreover, in comparison with the Capan-1 cells, the HCT116 cells are more sensitive to all of the compounds, and thus, we chose compound DC_517 for conducting apoptosis assays in HCT116 cells. The results demonstrated that DC_517 led to dose-dependent apoptotic cell death in HCT116 cells (Figure 6C).

Conclusion

DNA methylation as catalyzed by DNMTs plays important roles in crucial cellular processes, such as embryonic development or differentiation, and it is involved in cancer development. Most DNMT inhibitors reported to date have low bioavailability and specificity. In the present study, we identified compound DC_05 as a novel inhibitor of DNMT1 with an IC_{50} value of 10.3 μM by using the docking-based virtual screening approach from a filtered small molecule SPECS compound database, which contains 198,745 compounds. DC_05 has shown remarkable selectivity towards other AdoMet-dependent protein methyltransferases (DNMT3A, DNMT3B, G9a, SUV39H1, MLL1, SET7/9 and PRMT1). Subsequently, similarity-based analog searching was conducted to select more potent compounds. On the basis of the structure of the selective inhibitor lead compound known as DC_05, 8 out of 19 DC_05 analogs were identified as micromolar DNMT1 inhibitors. The radioactive methylation assay results identified compounds DC_501 and DC_517 from this library of analogs as the two most potent DNMT1 inhibitors, with IC_{50} values of 2.5 μM and 1.7 μM, respectively. A Surface Plasmon Resonance-based binding assay precisely validated these potential DNMT1 inhibitors by measuring direct interactions between DNMT1 and the compounds. The equilibrium dissociation constant (K_D) between DC_05 and DNMT1 is approximately 1.09 μM, and that of DC_517 is 0.91 μM, verifying the tight binding of these compounds with DNMT1. It should be noted that these DC_05 analogs are chiral compounds, and our purchased samples are in racemic form. To investigate how the chirality affects the activity of these compounds, asymmetric syntheses were performed to obtain all DC_05 and DC_517 enantiomers, and their enzymatic assays revealed no obvious activity differences between the enantiomers and their corresponding racemates. Our molecular docking studies show that the binding poses of the two enantiomers with DNMT1 closely resemble one another, which is consistent with their activity assay results. This finding suggests that the chiral structures of the compounds do not influence its activities. Furthermore, when tested on HCT116 and Capan-1 cells, DC_05, DC_501 and DC_517 can significantly block the proliferation of cells at a low micromolar concentration.

Given that the enantiomers show a similar potency against DNMT1 in biochemical assays, they also display the same level of anti-proliferative activities in their corresponding racemates in cell-based studies. Moreover, the most potent inhibitor, which was compound DC_517, induced dose-dependent apoptotic cell death in HCT116 cells.

Taken together, our experiments used virtual screening and similarity searching to find novel potent non-nucleoside DNMT1 inhibitors with considerable specificity for DNMT1. We identified the compounds that are selective and highly potent inhibitors of DNMT1 via biochemical and cellular assays. Unlike the nucleoside compounds, the DC_05-inhibiting activity against DNMT1 is a result of binding to DNMT1 instead of incorporating into DNA. The SAR analysis and predicted binding mode studies of these analogs show that a better occupation of the cytosine and SAM pockets is beneficial for the higher inhibitory activity of inhibitors and that the formation of ionic interactions and/or hydrogen bonds in linking the two pockets is necessary to form an interaction between the compounds and the DNMT1. In addition, the SAM pocket shows a high affinity to hydrophobic groups. These results may provide meaningful clues for the future structural optimization of these compounds and lay the foundation for the further development of DNMT1 inhibitors with greater potency and specificity for cancer therapy.

Experimental Section

Virtual Screening Protocol.

Preparing the Protein Structure. The crystal structure of murine DNMT1 that was resolved with the SAH and DNA substrate was retrieved from the Protein Data Bank (PDB access number 4DA4). Specifically, DNA fragments and the solvent molecules were deleted. The remaining protein structure was prepared using the Protein Preparation Wizard module (Schrödinger, LLC: New York, NY, 2010) in the Maestro program (Maestro version 9.1; Schrödinger, LLC: New York, NY, 2010) with standard Glide protocols.[43] In brief, the hydrogen atoms were properly added to the complexes, bond corrections were applied to the co-crystallized

ligand, the hydrogen bond networks and flip orientations/tautomeric states of Gln, Asn, and His residues were optimized to maximize hydrogen bond formation, and an exhaustive sampling was performed with regards to hydrogen bond assignment. Finally, a restrained minimization on the ligand-protein complexes was performed with the OPLS_2005 force field and the default value for RMSD of 0.30 Å for non-hydrogen atoms was used.

Preparing the Ligand Database. A SPECS database containing 198,745 compounds was used as a ligand database. The ligands were first filtered in Pipeline Pilot V7.5 (Pipeline Pilot, Accelrys Software Inc.: San Diego, CA) to remove the molecules with unfavorable physicochemical properties, such as those containing rare atoms (B, Si, Ni, Ti, Se and others), molecular weights larger than 450 and water solubility values (logS) larger than -1 or smaller than -6. After the possibilities were filtered, there were 111,121 compounds remaining. The three-dimensional (3D) coordinates and all the stereoisomers of the ligands were generated with LigPrep (LigPrep 2.4; Schrödinger, LLC: New York, NY, 2010), and their protonation states were determined at a target pH 7.0 ± 2.0 with Epik in its default mode (Epik 2.1; Schrödinger, LLC: New York, NY, 2010). The resulting structures were used as the starting point for all docking simulations.

Glide Docking Procedure. The Glide program was used to generate the grid file. The receptor grid was defined as an enclosing box centered at the native ligand SAH to include the cofactor and substrate. Docking was performed using Glide software (Glide 5.6, Schrödinger, LLC: New York, NY, 2010) with the standard precision (SP) mode first, and then the top 10000 poses were re-docked with the extra precision (XP) mode. Top-ranked compounds with GScores lower than -6.0 were then left for structural clustering with Pipeline Pilot V7.5, in which the average number of molecules that each cluster contains was set to 20. Finally, the compounds representing cluster centers were extracted and ranked according to their GScores, and then the top-ranked 51 structurally diverse compounds were selected for purchase from SPECS Corp. (The Netherlands). The putative binding modes of DC_05 analogs were all generated using Glide in XP mode.

Plasmid Construction, Protein Expression and Purification.

Sequence coding residues 731-1602 of mouse DNMT1 (mDNMT1) were cloned into a modified pET28a, which encodes a SUMO tag after the N-terminal His_6 tag. The mDNMT1 protein was expressed in *E. coli* BL21 (DE3) RIL cells. The cells were grown in L.B. (Luria-Bertani broth) at 37°C. When the $O.D_{600}$ reached 0.6, the temperature was shifted to 15°C, and the cells were induced with 0.4 mM IPTG (isopropyl β-D-1-thiogalactopyranoside) for 16 h. The protein was first purified through a HisTrap FF column (GE Healthcare), and then, the His_6-SUMO tag was removed by ULP1 at 4°C overnight. After that, the mDNMT1 protein was further purified through a Heparin HP column (GE Healthcare), followed by gel-filtration chromatography on a Superdex 200 10/300 column (GE Healthcare). The purified mDNMT1 protein was stored at -80°C in buffer containing 50 mM Tris-HCl (pH 8.0), 200 mM NaCl, 5 mM DTT, 5% glycerol and 1 mM $MgSO_4$.

DNMT3A/DNMT3L, MLL1, DNMT3B, SUV39H1, SET7/9 and G9a were purchased from Shanghai Chempartner Co., Ltd.

DNMT1 Inhibition Assays.

ELISA DNMT1 Activity Assay. All the compounds were first screened using an ELISA EpiQuik DNA Methyltransferase (DNMT) Activity/Inhibitor Assay Kit (Epigentek). To measure the effects of the compounds on mouse DNMT1 activity, 200 nM purified DNMT1 was incubated with 200 μM of the different compounds and *S*-adenosylmethionine (AdoMet) in the DNMT assay buffer in the assay plate at 37°C for 2 h.[44] Next, every sample was incubated with the capture and detection antibody, followed by incubation with developer solution for 10 mins at room temperature. The absorbance was measured at 450 nm using a POLARstar Omega microplate reader (BMG). *S*-Adenosylhomocysteine (AdoHcy) was used as a positive control.

Radioactive Methylation Assay. The DNMT1 radioactive methylation inhibition assays were performed in

30 μL reactions containing 0.1 μM adenosyl-L-methionine S-[methyl-^{3}H] (^{3}H-SAM,15 Ci/mmol, Perkin Elmer), 0.25 μg/mL poly (dI-dC) · poly (dI-dC) (Sigma), 40 nM of DNMT1 in 50 mM Tris-HCl pH 8.0, 1 mM DTT, 5% glycerol and 100 μg/mL BSA. The proteins were pre-incubated with a range of compound concentrations for 15 mins at room temperature before adding the substrate and [^{3}H]-SAM. After 60 mins of incubating at 37°C, the reaction systems were transferred to a MultiScreen HTS Filter Plate (Millipore), and the plate was washed 3 times with ddH_2O via vacuum. The radioactivity was determined by liquid scintillation counting (MicroBeta, Perkin Elmer). IC_{50} values were derived by fitting the data for the inhibition percentage to a dose response curve by nonlinear regression in GraphPad Prism 5.0.

Methyltransferase Enzymatic Selectivity Assay

The DNMT3A/DNMT3L and DNMT3B/DNMT3L radioactive methylation inhibition assays were similar to that of DNMT1, using 10 nM synthetic biotinylated DNA oligonucleotides (Life Technologies) as a substrate. Sixty nM of DNMT3A/DNMT3L (BPS, 51106) or 25 nM DNMT3B/DNMT3L (BPS, 51104) was pre-incubated with various compound concentrations for 15 mins at room temperature before the substrate and [^{3}H]-SAM were added. After 4 hours of incubation at room temperature, the reaction systems were transferred to a 384-well streptavidin-coated Flashplate Microplate (PerkinElmer) and then incubated for 1 hr at room temperature. The radioactivity was also determined by liquid scintillation counting (MicroBeta, Perkin Elmer).

Methylation inhibition assays for MLL1, SUV39H1, SET7/9, and G9a were performed in modified Tris pH 9.0 buffer using AlphaLisa technology. Ten μL of the reaction system contained a corresponding concentration of SAM (Sigma) (MLL1 2 μM, SUV39H1 20 μM, SET7/9 0.22 μM and G9a 50 μM), which was the Km value in each enzymatic reaction, plus 100 nM biotinylated peptide H3 (1-21) (synthesis by GLChina) and the relevant enzyme concentration (2 nM MLL1, 3 nM SUV39H1, 0.2 nM SET7/9, and 0.03 nM G9a). Methylation inhibition assays for PRMT1 are similar to those of other methyltransferases in

modified Tris pH 8.0 buffer. The reaction system contained 0.8 μM SAM, 50 nM biotinylated peptide H4 (1-21) S1ac (synthesis by GLChina) and 0.1 nM PRMT1. The proteins were pre-incubated with various compound concentrations for 15 mins at room temperature before the substrate and SAM were added. After 60 mins of incubation at room temperature, acceptor and donor AlphaLisa beads were added according to the manufacturer's recommendations. The signals were read in Alpha mode with an EnSpire Multimode Plate Reader (PerkinElmer). IC_{50} values were derived by fitting the data for the inhibition percentage to a dose-response curve by nonlinear regression in GraphPad Prism 5.0.

Surface Plasmon Resonance (SPR)-Based Binding Assays

The SPR binding assays were performed on a Biacore T200 instrument (GE Healthcare) at 25°C as described.[28] DNMT1 protein was covalently immobilized on a CM5 chip using a standard amine-coupling procedure in 10 mM sodium acetate (pH 5.0). The chip was first equilibrated with HBS-EP buffer (10 mM HEPES (pH 7.4), 150 mM NaCl, 3 mM EDTA, 0.05% (v/v) surfactant P20, and 0.1% (v/v) DMSO) overnight. The compounds were serially diluted with HBS-EP buffer and injected for 120 s (contact phase), followed by 120 s (dissociation phase). The K_D values of the tested compounds were determined by Biacore T200 evaluation software (GE Healthcare).

Chemistry

Reagents were purchased from commercial sources and used as received. All anhydrous reactions were performed under a nitrogen atmosphere. DMF was distilled from CaH_2 prior to use. Melting points (uncorrected) were determined on an XRC-1 micro melting point apparatus. IR spectra were recorded on a PerkinElmer Spectrum Two FT-IR. An HRMS was taken on a ThermoFisher LTQ Orbitrap XL instrument. The ^1H and ^{13}C NMR experiments were performed on a Bruker AM-400 spectrometer. The purities of all tested compounds were determined by an HPLC (Agilent Technologies 1200 series) equipped with a C-18 bounded-phase column (Waters Symmetry C18, 4.6 mm × 250 mm, 5 um). A gradient elution was

performed with MeOH and water as a mobile phase, and the results were monitored at 254 nm. All tested compounds were >95% pure.

Synthetic method for compounds (*R*)-DC_05

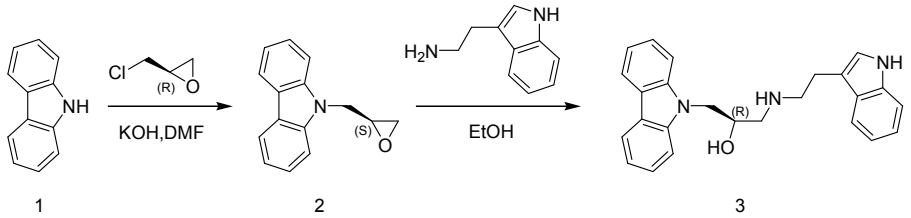

(S)-9-(oxiran-2-ylmethyl)-9H-carbazolyl (1). Powdered KOH (0.434 g, 6.85 mmol) was added to a carbazole solution (1.000 g, 5.98 mmol) in DMF (6.0 mL) at ambient temperature and stirred for 30 min until dissolved. (*R*)-(-)-Epichlorohydrin (0.94 mL, 11.97 mmol) was added via syringe and the reaction was stirred at room temperature overnight. Upon completion, the solution was partitioned between EtOAc and H_2O. The aqueous layer was extracted by EtOAc, and the combined organics were washed with saturated aqueous NaCl, dried over Na_2SO_4, filtered, and concentrated in vacuo. The crude residue was recrystallized from EtOAc/Hexane to yield compound 2 (475 mg, 35%).

Its characteristics were as follows: mp 75-77°C; IR (neat) 3051, 2995, 1594, 1483, 1452, 1324, 1217, and 1152 cm^{-1}; HRMS-ESI: calcd for $C_{15}H_{14}NO$ $[M+H]^+$ 224.0997, found 224.1064; ^1H NMR ($CDCl_3$, 400 MHz) δ 8.12 (2H, s), 7.48 (4H, s), 7.29 (2H, s), 4.62-4.58 (1H, m), 4.39-4.35 (1H, m), 3.33 (1H, s), 2.79-2.78 (1H, d, $J = 0.4$), and 2.56 (1H, s), ^{13}C NMR ($CDCl_3$, 100 MHz) δ140.83 (2C), 125.99 (2C), 123.13 (2C), 120.44 (2C), 119.48 (2C), 108.90 (2C), 50.64, 45.39, and 44.68.

(R)-1-((2-(1H-indol-3-yl)ethyl)amino)-3-(9H-carbazol-9-yl)propan-2-ol (3). A solution of compound 2 (242 mg, 1.08 mmol) and tryptamine (720 mg, 4.34 mmol) in ethanol (10 mL) was stirred at room temperature overnight. After the complete consumption of compound 2 (TLC), the solvent was evaporated to dryness, and the residue was purified by chromatography (SiO_2, 100% EtOAc) to produce compound 3 as a white solid (177 mg, 44%).

Its characteristics were as follows: mp 151-153°C; IR (neat) 3275, 3013, 2937, 1597, 1450, 1351, 1324, 1205, and 1111 cm^{-1}; HRMS-ESI: calcd for $C_{25}H_{26}N_3O$ $[M+H]^+$ 384.1998, found 384.2066. ^1H NMR (DMSO-d_6, 400 MHz) δ 10.79 (1H, s), 8.13-8.11 (2H, d, *J* = 0.8), 7.63-7.61 (2H, d, *J* = 0.8), 7.53-7.51 (1H, d, *J* = 0.8), 7.43-7.39 (2H, t, *J* = 0.8), 7.35-7.33 (1H, d, *J* = 0.8), 7.20-7.15 (3H, m), 7.08-7.05 (1H, t, *J* = 0.8), 6.99-6.95 (1H, t, *J* = 0.8), 5.04 (1H, brs), 4.50-4.45 (1H, m), 4.31-4.26 (1H, m), 4.03-4.01 (1H, t, *J* = 0.8), 2.85-2.82 (4H, m), 2.66-2.49 (2H, m), and 2.05 (1H, brs) ^{13}C NMR (DMSO-d_6, 100 MHz) δ140.60 (2C), 136.27, 127.30, 125.46 (2C), 122.56, 122.01, 120.80, 119.99(2C), 118.57 (2C), 118.30, 118.12, 112.57, 111.32, 109.71 (2C), 68.80, 53.04, 50.32, 47.06, and 25.55.

Synthetic method for compounds (*S*)-DC_05

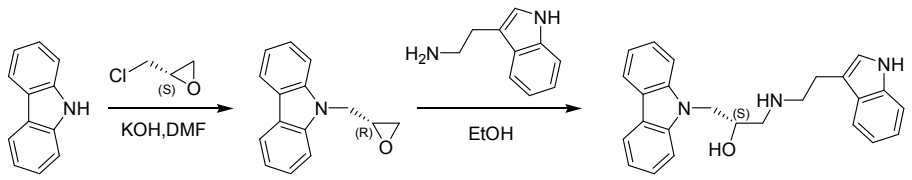

1 4 5

(R)-9-(oxiran-2-ylmethyl)-9H-carbazole (4). Powdered KOH (0.434 g, 6.85 mmol) was added to a carbazole solution (1.000 g, 5.98 mmol) in DMF (6.0 mL) at ambient temperature and stirred for 30 min until dissolved. (*S*)-(+)-Epichlorohydrin (0.94 mL, 11.97 mmol) was added via syringe and the reaction was stirred at room temperature overnight. Upon completion, the solution was partitioned between EtOAc and H_2O. The aqueous layer was extracted by EtOAc, and the combined organics were washed with saturated aqueous NaCl, dried over Na_2SO_4, filtered, and concentrated in vacuo. The residue was purified by chromatography (SiO_2, 4% EtOAc/Hexane) to yield compound 4 as a white solid (423 mg, 32%).

The compounds were as follows: mp 72-74°C; IR (neat) 3052, 2996, 1594, 1483, 1452, 1324, 1217, and 1153 cm^{-1}; HRMS-ESI: calcd for $C_{15}H_{14}NO$ $[M+H]^+$ 224.0997, found 224.1066. ^1H NMR ($CDCl_3$, 400 MHz) δ 8.08-8.06 (2H, d, *J* = 0.8), 7.47-7.41 (4H, m), 7.25-7.20 (2H, m), 4.59-4.54 (1H, m), 4.36-4.30 (1H, m), 3.30-3.27 (1H, m), 2.76-2.74(1H, t, *J* = 0.4), and 2.53-2.51 (1H, m), ^{13}C NMR ($CDCl_3$, 100 MHz) δ140.84

(2C), 126.01 (2C), 123.14 (2C), 120.46 (2C), 119.50 (2C), 108.90(2C), 50.66, 45.42, and 44.70.

(S)-1-((2-(1H-indol-3-yl)ethyl)amino)-3-(9H-carbazol-9-yl)propan-2-ol (5). A solution of compound 4 (223 mg, 1.00 mmol) and tryptamine (640 mg, 4.00 mmol) in ethanol (10 mL) was stirred at room temperature overnight. After the complete consumption of compound 4 (TLC), the solvent was evaporated to dryness, and the residue was purified by chromatography (SiO_2, 100% EtOAc) to afford compound 5 as a white solid (165 mg, 41%).

It had the following characteristics: mp 158-160°C; IR 3275, 3013, 2908, 1597, 1450, 1351, 1324, 1205, and 1111 cm^{-1}; HRMS-ESI: calcd for $C_{25}H_{26}N_3O$ $[M+H]^+$ 384.1998, found 384.2066. ^1H NMR (DMSO-d_6, 400 MHz) δ 10.79 (1H, s), 8.13-8.11 (2H, d, *J* = 0.8), 7.63-7.61 (2H, d, *J* = 0.8), 7.53-7.51 (1H, d, *J* = 0.8), 7.43-7.39 (2H, t, *J* = 0.8), 7.35-7.33 (1H, d, *J* = 0.8), 7.20-7.15 (3H, m), 7.08-7.05 (1H, t, *J* = 0.8), 6.99-6.95 (1H, t, *J* = 0.8), 5.04 (1H, brs), 4.50-4.45 (1H, m), 4.31-4.26 (1H, m), 4.03-4.01 (1H, t, *J* = 0.8), 2.85-2.82 (4H, m), 2.66-2.49 (2H, m), and 2.05 (1H,brs) ^{13}C NMR (DMSO-d_6, 100 MHz) δ140.59 (2C), 136.26, 127.29, 125.45 (2C), 122.55, 122.00, 120.79, 119.98(2C), 118.57 (2C), 118.29, 118.11, 112.55, 111.31, 109.70 (2C), 68.79, 53.02, 50.31, 47.05, and 25.54.

Synthetic method for compounds (*R*)-DC_517

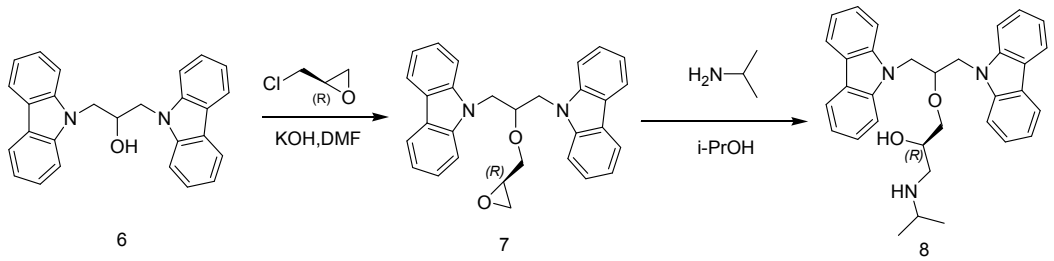

(R)-9,9'-(2-(oxiran-2-ylmethoxy)propane-1,3-diyl)bis(9H-carbazole) (7). To the solution of compound 6 (1 g, 2.56 mmol) in 20 mL of acetone, 2.4 g (25.6 mmol) of (*R*)-2-(chloromethyl)oxirane, 0.5 g (7.68 mmol) of 85% powdered KOH and 0.37 g (2.56 mmol) of anhydrous Na_2SO_4 were added. The mixture was stirred at room temperature until compound 6 was completely consumed. The mixture was treated with EtOAc and

water. The organic layer was washed with distilled water until the wash water was neutral, and it was dried over anhydrous Na_2SO_4 and filtered off. EtOAc was removed and the residue was crystallized with 40 mL of petrol ether/EtOAc (10:1) to yield (*R*)-9,9'-(2-(oxiran-2-ylmethoxy)propane-1,3-diyl)bis(9*H*-carbazole) (7) as a white solid (910 mg, 79.7%).

The compound had the following characteristics: mp 143-144°C; IR (neat) 3049, 2934, 2863, 1626, 1594, 1485, 1452, 1326, 1222, 1153, 1120, and 1061 cm^{-1}; HRMS-ESI: calcd for $C_{30}H_{27}N_2O_2$ $[M+H]^+$ 447.2073, found 447.2060. ^1H NMR ($CDCl_3$, 400 MHz) δ8.09-8.04 (4H, m), 7.42-7.29 (6H, m); 7.24-7.18 (6H, m), 4.57-4.46 (2H, m), 4.37-4.29 (2H, m), 4.25-4.20 (1H, m), and 3.06-3.02 (1H, m); 2.98-2.94 (1H, m); 2.50-2.47 (1H, m), 2.33-2.31 (1H, t, J = 0.4); and 2.04-2.02 (1H, m). ^{13}C NMR ($CDCl_3$, 100 MHz) δ140.56, 140.53, 126.08 (2C), 125.99 (2C), 123.22, 123.13, 120.57 (2C), 120.49 (2C), 119.56 (2C), 119.48(2C), 109.00(8C), 78.59, 72.59, 50.39, 46.01(2C), and 44.32.

(R)-1-((1,3-di(9H-carbazol-9-yl)propan-2-yl)oxy)-3-(isopropylamino)propan-2-ol (8). A solution of epoxide 7 (300 mg, 0.67 mmol) and isopropylamine (395 mg, 6.71 mmol, 10 equiv.) in isopropanol 4 mL was heated to reflux for 1 h. After the complete consumption of the epoxide 7 (TLC), the solvent was evaporated to dryness, and the crude product was purified by flash column chromatography on silica gel (EtOAc/MeOH 20:1 as eluent) to afford (*R*)-1-((1,3-di(9*H*-carbazol-9-yl)propan-2-yl)oxy)-3-(isopropylamino)propan-2-ol(8) as a white solid (161 mg, 47%).

The compound had the following characteristics: mp 108-110°C; IR(neat) 3627, 3303, 3049, 2930, 2868, 1626, 1595, 1484, 1452, 1325, 1223, 1153, 1120, and 1061 cm^{-1}; HRMS-ESI: calcd for $C_{33}H_{36}N_3O_2$ $[M+H]^+$ 506.2808, found 506.2792. ^1H NMR ($CDCl_3$, 400 MHz) δ8.08-8.06 (4H, d, J = 0.8), 7.39-7.37 (4H, d, J = 0.8); 7.26-7.20 (8H, m), 4.55-4.50 (2H, m), 4.36-4.27 (2H, m), 3.22-3.18 (1H, m), 3.04-2.99 (2H, m); 2.47-2.41(1H, m), 2.12-1.98 (2H, m), 1.85 (2H, brs), and 0.87-0.85 (6H, d, J = 0.8). ^{13}C NMR ($CDCl_3$, 100

MHz) δ140.54 (2C), 126.06 (4C), 123.18 (2C), 120.65 (3C), 120.62 (3C), 119.56 (4C), 108.88 (3C), 108.82 (3C), 78.50, 74.35, 69.03, 44.81, 44.74, 45.75, 45.70, 22.90, and 22.83.

Synthetic method for compounds (*S*)-DC_517

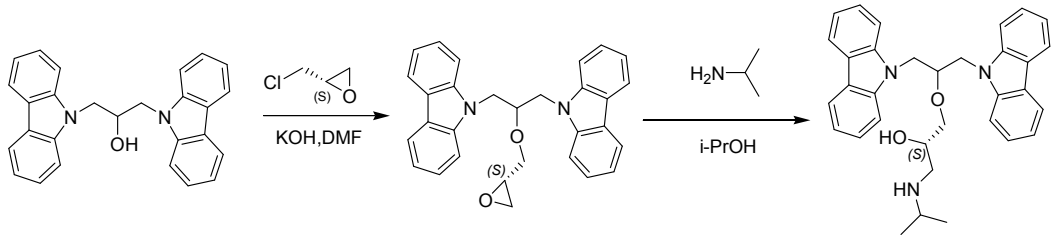

(S)-9,9'-(2-(oxiran-2-ylmethoxy)propane-1,3-diyl)bis(9H-carbazole) (9). To the solution of compound 6 (1 g, 2.56 mmol) in 20 mL of acetone 2.4 g (25.6 mmol) of (S)-2-(chloromethyl)oxirane, 0.5 g (7.68 mmol) of 85% powdered KOH and 0.37 g (2.56 mmol) of anhydrous Na_2SO_4 were added. The mixture was stirred at room temperature until compound 6 was completely consumed. The mixture was treated with EtOAc and water. The organic layer was washed with distilled water until the wash water was neutral, and it was dried over anhydrous Na_2SO_4 and filtered off. The EtOAc was removed and the residue was crystallized with 40 mL of petrol ether/EtOAc (10:1) to give (S)-9,9'-(2-(oxiran-2-ylmethoxy)propane-1,3-diyl)bis(9H-carbazole) (9) as a white solid (840 mg, 73.6%).

The characteristics were as follows: mp 142-144°C; IR (neat) 3049, 2934, 2863, 1626, 1594, 1485, 1452, 1326, 1222, 1153, 1120, and 1061 cm^{-1}; HRMS-ESI: calcd for $C_{30}H_{27}N_2O_2$ $[M+H]^+$ 447.2072, found 447.2060. ^1H NMR ($CDCl_3$, 400 MHz) δ8.09-8.04 (4H,m), 7.42-7.29 (6H, m), 7.24-7.18 (6H, m), 4.57-4.46 (2H, m), 4.37-4.29 (2H, m), 4.25-4.20 (1H, m), 3.06-3.02 (1H, m); 2.98-2.94 (1H, m); 2.49-2.47 (1H, m), 2.33-2.31 (1H, t, J = 0.4); and 2.04-2.02 (1H, m). ^{13}C NMR ($CDCl_3$, 100 MHz) δ140.56 (2C), 126.08 (2C), 125.99 (2C), 123.21, 123.13, 120.57 (2C), 120.49 (2C), 119.56 (2C), 119.48 (2C),109.00 (8C), 78.58, 72.59, 50.39, 46.00 (2C), and 44.31.

(S)-1-((1,3-di(9H-carbazol-9-yl)propan-2-yl)oxy)-3-(isopropylamino)propan-2-ol (10). A solution of

epoxide 9 (300 mg, 0.67 mmol) and isopropylamine (395 mg, 6.71 mmol, 10 equiv.) in isopropanol 4 mL was heated to reflux for 1 h. After the complete consumption of epoxide 9 (TLC), the solvent was evaporated to dryness, and the crude product was purified by flash column chromatography on silica gel (EtOAc/MeOH 20:1 as eluent) to afford (S)-1-((1,3-di(9H-carbazol-9-yl)propan-2-yl)oxy)-3-(isopropylamino)propan-2-ol(10) as a white solid (150 mg, 44%).

The characteristics were as follows: mp 91-93°C; IR (neat) 3627, 3303, 3049, 2930, 2868, 1626, 1595, 1484, 1452, 1325, 1223, 1153, 1120, and 1061 cm^{-1}. HRMS-ESI: calcd for $C_{33}H_{36}N_3O_2$ $[M+H]^+$ 506.2807, found 506.2791. ^1H NMR ($CDCl_3$, 400 MHz) δ8.08-8.06 (4H, d, *J* = 0.8), 7.39-7.37 (4H, d, *J* = 0.8); 7.25-7.20 (8H, m), 4.55-4.50 (2H, m), 4.37-4.28 (2H, m), 3.24-3.22 (1H, m), 3.07-2.99 (2H, m); 2.47-2.41(1H, m), 2.14-1.99 (4H, m); and 0.88-0.86 (6H, d, *J* = 0.8). ^{13}C NMR ($CDCl_3$, 100 MHz) δ140.54(2C), 126.07(4C), 123.18(2C), 120.65(3C), 120.62 (3C), 119.57 (4C), 108.89 (3C), 108.83 (3C), 78.49, 74.29, 68.87, 44.89, 44.78, 45.75, 45.69, 22.70, 22.64, 46.00 (2C), and 44.31.

Cell culture, cell proliferation assays and flow cytometry assays

HCT116 (colon cancer) and Capan-1 (pancreatic cancer) cell lines were purchased from the American Type Culture Collection (ATCC) and were maintained in McCoy's 5A and DMEM (Life technologies) supplemented with 10% fetal bovine serum (Life Technologies). The cells were cultured at 37°C in a humidified atmosphere of 5% CO_2 in a CO_2 incubator. The compounds were dissolved in DMSO and stored at -20°C. Control cells were treated with media containing an equal concentration of DMSO. For the cell proliferation assay, cells were treated with different compound concentrations. HCT116 and Capan-1 cell viabilities were measured by MTT assay, and the absorbance was measured at 490 nm. The percent proliferation was calculated by normalizing the absorbance to that of the control cells.

The cell apoptosis was determined by dual staining with 7-amino-actinomycin (7-AAD) and annexin V

conjugated to phycoerythrin (PE) (BD Pharmingen). HCT116 cells were treated with 0, 0.75, 1.5 and 3 μM DC_517 for 24 hours, and then 1×10^6 cells were stained with annexin V-PE and 7-AAD for 15 mins away from the light and analyzed by flow cytometry using a LSR II cytometer (BD Pharmingen). Annexin V+ and/or 7-AAD+ cells were identified as apoptotic, and cells excluding both annexin V-PE and 7-AAD were considered viable. The annexin V-/PI- cells that were normalized to untreated controls are represented as a percentage of live cells.

Associated content:

Supporting Information

A validation of the molecular docking; Agarose gel electrophoresis assay for compounds; The chemical structure and Glide Score for 51 compounds selected from virtual screening; Biochemical assays for DC_05 against DNMT3A, DNMT3B, G9a, SUV39H1, MLL1, SET7/9 and PRMT1; A sequence alignment of the catalytic site of DNMT1, DNMT3A, PRMT1, G9a, MLL1 and SET7/9; Superimposition of the catalytic domains of PRMT1, DNMT3a and DNMT1 with (*R*)-DC_05 and (*S*)-DC_05 in cartoon mode; Dose-response plots for selected compounds DC_501, DC_503, DC_504, DC_508, DC_512, DC_514, DC_516 and DC_517 against DNMT1; The 2D ligand interaction diagram of enantiomers of DC_05 and DC_517; The 2D ligand interaction diagram of DC_512, DC_504 and DC_508; and the cellular activity of DC_05, (*R*)-DC_05, (*S*)-DC_05, DC_517, (*R*)-DC_517 and (*S*)-DC_517. This material is available free of charge via the Internet at http://pubs.acs.org.

ACKNOWLEDGMENT

This work was supported by the Hi-Tech Research and Development Program of China (2012AA020302 to CL), the National Natural Science Foundation of China (21210003 and 81230076 to HJ，81430084 to MZ, 81202398 to BL, 21472208 and 91229204 to CL) and the National Science and Technology Major Project "Key New Drug Creation and Manufacturing Program" (2014ZX09507002-005-012 to MZ).

ABBREVIATIONS USED

μ, micro; μM, micromole per liter; °C, degrees Celsius; 2D, two dimensional; 3D, three dimensional; 7-AAD , 7-amino-actinomycin ; AdoHcy, *S*-Adenosylhomocysteine; AdoMet, *S*-adenosylmethionine; ATCC, American Type Culture Collection; DMEM, dulbecco's modified eagle medium; DMSO, dimethyl sulfoxide; DNA, deoxyribonucleic acid; DNMT, DNA methyltransferase; DNMT1, DNA methyltransferase 1; DNMT3A, DNA methyltransferase 3A; DNMT3B, DNA methyltransferase 3B; DTT，dithiothreitol；EDTA, ethylenediaminetetraacetic acid; ELISA , enzyme-linked immunosorbent assay; FDA, Food and Drug Administration; GScores, Glide Scores; h, hour; HEPES, 4-(2-hydroxyethyl)-1-piperazineethanesulfonic acid; ^{3}H-SAM, Adenosyl-L-methionine S-[methyl-^{3}H]; IC_{50}, half-maximum inhibitory concentration; IPTG, Isopropyl β-D-1-thiogalactopyranoside; K_D, equilibrium dissociation constant; L.B., Luria-Bertani; mM, millimole per liter; min, minute; MTT, (3-(4,5-Dimethylthiazol-2-yl)-2,5-diphenyltetrazolium bromide; nM, nanomole per liter; nm, nanometer; PDB, Protein Data Bank; RMSD, root-mean square deviation; PRMT1, protein arginine N-methyltransferase 1; SAH, S-Adenosyl-L-homocysteine; SAM, S-adenosyl-L-methionine; SAR, structure-activity relationship; S P, standard precision; SPR, surface plasmon resonance; Tris, tris(hydroxymethyl)aminomethane; TSGS, tumor suppressor genes; XP, extra precision;

Reference：

1. Yoo, C. B.; Jones, P. A. Epigenetic therapy of cancer: past, present and future. *Nat Rev Drug Discov* **2006,** *5*, 37-50.

2. Esteller, M. Epigenetics in cancer. *N Engl J Med* **2008,** *358*, 1148-1159.

3. Suzuki, T.; Tanaka, R.; Hamada, S.; Nakagawa, H.; Miyata, N. Design, synthesis, inhibitory activity, and binding mode study of novel DNA methyltransferase 1 inhibitors. *Bioorg Med Chem Lett* **2010,** *20*, 1124-1127.

4. Siedlecki, P.; Garcia Boy, R.; Musch, T.; Brueckner, B.; Suhai, S.; Lyko, F.; Zielenkiewicz, P. Discovery of two novel, small-molecule inhibitors of DNA methylation. *J Med Chem* **2006,** *49*, 678-683.

5. Jones, P. A.; Baylin, S. B. The epigenomics of cancer. *Cell* **2007**, *128*, 683–692.

6. Goll, M. G.; Bestor, T. H. Eukaryotic cytosine methyltransferases. *Annu Rev Biochem* **2005,** *74*, 481-514.

7. Bestor, T. H. The DNA methyltransferases of mammals. *Hum Mol Genet* **2000,** *9*, 2395-2402.

8. Leonhardt, H.; Page, A. W.; Weier, H. U.; Bestor, T. H. A targeting sequence directs DNA methyltransferase to sites of DNA replication in mammalian nuclei. *Cell* **1992,** *71*, 865-873.

9. Castellano, S.; Kuck, D.; Viviano, M.; Yoo, J.; Lopez-Vallejo, F.; Conti, P.; Tamborini, L.; Pinto, A.; Medina-Franco, J. L.; Sbardella, G. Synthesis and biochemical evaluation of delta(2)-isoxazoline derivatives as DNA methyltransferase 1 inhibitors. *J Med Chem* **2011,** *54*, 7663-7677.

10. Egger, G.; Liang, G.; Aparicio, A.; Jones, P. A. Epigenetics in human disease and prospects for epigenetic therapy. *Nature* **2004,** *429*, 457-463.

11. Stresemann, C.; Lyko, F. Modes of action of the DNA methyltransferase inhibitors azacytidine and decitabine. *Int J Cancer* **2008,** *123*, 8-13.

12. Gros, C.; Fahy, J.; Halby, L.; Dufau, I.; Erdmann, A.; Gregoire, J. M.; Ausseil, F.; Vispe, S.; Arimondo, P. B. DNA methylation inhibitors in cancer: recent and future approaches. *Biochimie* **2012,** *94*, 2280-2296.

13. Fang, M. Z.; Chen, D.; Sun, Y.; Jin, Z.; Christman, J. K.; Yang, C. S. Reversal of hypermethylation and reactivation of p16INK4a, RARbeta, and MGMT genes by genistein and other isoflavones from soy. *Clin Cancer Res* **2005,** *11*, 7033-7041.

14. Fang, M. Z.; Wang, Y.; Ai, N.; Hou, Z.; Sun, Y.; Lu, H.; Welsh, W.; Yang, C. S. Tea polyphenol (-)-epigallocatechin-3-gallate inhibits DNA methyltransferase and reactivates methylation-silenced genes in cancer cell lines. *Cancer Res* **2003,** *63*, 7563-7570.

15. Fagan, R. L.; Cryderman, D. E.; Kopelovich, L.; Wallrath, L. L.; Brenner, C. Laccaic acid A is a direct,

DNA-competitive inhibitor of DNA methyltransferase 1. *J Biol Chem* **2013,** *288*, 23858-23867.

16. Zambrano, P.; Segura-Pachero, B.; Perez-Cardenas, E.; Cetina, L.; Revilla-Vazquez, A. R.; Taja-Chayeb, L. A. T.; Chavez-Blanco, A.; Angeles, E.; Cabrera, G.; Sandoval, K.; Trejo-Becerril, C.; Chanona-Vilchis, J.; Duenas-Gonzalez, A. A phase I study of hydralazine to demethylate and reactivate the expression of tumor suppressor genes. *Bmc Cancer* **2005,** *5*, 44-56.

17. Villar-Garea, A.; Fraga, M. F.; Espada, J.; Esteller, M. Procaine is a DNA-demethylating agent with growth-inhibitory effects in human cancer cells. *Cancer Res* **2003,** *63*, 4984-4989.

18. Cornacchia, E.; Golbus, J.; Maybaum, J.; Strahler, J.; Hanash, S.; Richardson, B. Hydralazine and procainamide inhibit T-cell DNA methylation and induce autoreactivity. *J immunol* **1988,** *140*, 2197-2200.

19. Brueckner, B.; Garcia Boy, R.; Siedlecki, P.; Musch, T.; Kliem, H. C.; Zielenkiewicz, P.; Suhai, S.; Wiessler, M.; Lyko, F. Epigenetic reactivation of tumor suppressor genes by a novel small-molecule inhibitor of human DNA methyltransferases. *Cancer Res* **2005,** *65*, 6305-6311.

20. Datta, J.; Ghoshal, K.; Denny, W. A.; Gamage, S. A.; Brooke, D. G.; Phiasivongsa, P.; Redkar, S.; Jacob, S. T. A new class of quinoline-based DNA hypomethylating agents reactivates tumor suppressor genes by blocking DNA methyltransferase 1 activity and inducing its degradation. *Cancer Res* **2009,** *69*, 4277-4285.

21. Seidel, C.; Florean, C.; Schnekenburger, M.; Dicato, M.; Diederich, M. Chromatin-modifying agents in anti-cancer therapy. *Biochimie* **2012,** *94*, 2264-2279.

22. Chuang, J. C.; Yoo, C. B.; Kwan, J. M.; Li, T. W. H.; Liang, G. N.; Yang, A. S.; Jones, P. A. Comparison of biological effects of non-nucleoside DNA methylation inhibitors versus 5-aza-2 '-deoxycytidine. *Mol Cancer Ther* **2005,** *4*, 1515-1520.

23. Stresemann, C.; Brueckner, B.; Musch, T.; Stopper, H.; Lyko, F. Functional diversity of DNA methyltransferase inhibitors in human cancer cell lines. *Cancer Res* **2006,** *66*, 2794-2800.

24. Valente, S.; Liu, Y. W.; Schnekenburger, M.; Zwergel, C.; Cosconati, S.; Gros, C.; Tardugno, M.; Labella, D.; Florean, C.; Minden, S.; Hashimoto, H.; Chan, Y. Q.; Zhang, X.; Kirsch, G.; Novellino, E.;

Arimondo, P. B.; Miele, E.; Ferretti, E.; Gulino, A.; Diederich, M.; Cheng, X. D.; Mai, A. Selective non-nucleoside inhibitors of human DNA methyltransferases active in cancer Including in cancer stem cells. *J Med Chem* **2014,** *57*, 701-713.

25. Asgatay, S.; Champion, C.; Marloie, G.; Drujon, T.; Senamaud-Beaufort, C.; Ceccaldi, A.; Erdmann, A.; Rajavelu, A.; Schambel, P.; Jeltsch, A.; Lequin, O.; Karoyan, P.; Arimondo, P. B.; Guianvarc'h, D. Synthesis and evaluation of analogues of N-Phthaloyl-L-tryptophan (RG108) as inhibitors of DNA methyltransferase 1. *J Med Chem* **2014,** *57*, 421-434.

26. Liang, Z.; Ding, X.; Ai, J.; Kong, X.; Chen, L.; Chen, L.; Luo, C.; Geng, M.; Liu, H.; Chen, K.; Jiang, H. Discovering potent inhibitors against c-Met kinase: molecular design, organic synthesis and bioassay. *Org Biomol Chem* **2012,** *10*, 421-430.

27. Kong, X.; Qin, J.; Li, Z.; Vultur, A.; Tong, L.; Feng, E.; Rajan, G.; Liu, S.; Lu, J.; Liang, Z.; Zheng, M.; Zhu, W.; Jiang, H.; Herlyn, M.; Liu, H.; Marmorstein, R.; Luo, C. Development of a novel class of B-Raf(V600E)-selective inhibitors through virtual screening and hierarchical hit optimization. *Org Biomol Chem* **2012,** *10*, 7402-7417.

28. Chen, B.; Ye, F.; Yu, L.; Jia, G.; Huang, X.; Zhang, X.; Peng, S.; Chen, K.; Wang, M.; Gong, S.; Zhang, R.; Yin, J.; Li, H.; Yang, Y.; Liu, H.; Zhang, J.; Zhang, H.; Zhang, A.; Jiang, H.; Luo, C.; Yang, C. G. Development of cell-active N6-methyladenosine RNA demethylase FTO inhibitor. *J Am Chem Soc* **2012,** *134*, 17963-17971.

29. Wang, J.; Chen, L.; Sinha, S. H.; Liang, Z.; Chai, H.; Muniyan, S.; Chou, Y. W.; Yang, C.; Yan, L.; Feng, Y.; Li, K. K.; Lin, M. F.; Jiang, H.; Zheng, Y. G.; Luo, C. Pharmacophore-based virtual screening and biological evaluation of small molecule inhibitors for protein arginine methylation. *J Med Chem* **2012,** *55*, 7978-7987.

30. Li, K. K.; Luo, C.; Wang, D.; Jiang, H.; Zheng, Y. G. Chemical and biochemical approaches in the study of histone methylation and demethylation. *Med Res Rev* **2012,** *32*, 815-867.

31. Kuck, D.; Singh, N.; Lyko, F.; Medina-Franco, J. L. Novel and selective DNA methyltransferase inhibitors: Docking-based virtual screening and experimental evaluation. *Bioorgan Med Chem* **2010,** *18*, 822-829.

32. Medina-Franco, J.; Yoo, J. Docking of a novel DNA methyltransferase inhibitor identified from high-throughput screening: insights to unveil inhibitors in chemical databases. *Mol Divers* **2013,** *17*, 337-344.

33. Song, J. K.; Teplova, M.; Ishibe-Murakami, S.; Patel, D. J. Structure-based mechanistic insights into DNMT1-mediated maintenance DNA methylation. *Science* **2012,** *335*, 709-712.

34. Gaur, R.; Khan, R. A.; Tabassum, S.; Shah, P.; Siddiqi, M. I.; Mishra, L. Interaction of a ruthenium(II)-chalcone complex with double stranded DNA: Spectroscopic, molecular docking and nuclease properties. *J Photochem Photobiol* **2011,** *220*, 145-152.

35. Fornari, F. A.; Randolph, J. K.; Yalowich, J. C.; Ritke, M. K.; Gewirtz, D. A. Interference by doxorubicin with DNA unwinding in MCF-7 breast tumor cells. *Mol Pharmacol* **1994,** *45*, 649-656.

36. Milner, C. M.; Campbell, R. D. The G9a gene in the human major histocompatibility complex encodes a novel protein containing ankyrin-like repeats. *Biochem J* **1993,** *290*, 811-818.

37. Carbone, R.; Botrugno, O. A.; Ronzoni, S.; Insinga, A.; Di Croce, L.; Pelicci, P. G.; Minucci, S. Recruitment of the histone methyltransferase SUV39H1 and its role in the oncogenic properties of the leukemia-associated PML-retinoic acid receptor fusion protein. *Mol Cell Biol* **2006,** *26*, 1288-1296.

38. Dou, Y.; Milne, T. A.; Tackett, A. J.; Smith, E. R.; Fukuda, A.; Wysocka, J.; Allis, C. D.; Chait, B. T.; Hess, J. L.; Roeder, R. G. Physical association and coordinate function of the H3K4 methyltransferase MLL1 and the H4 K16 acetyltransferase MOF. *Cell* **2005,** *121*, 873-885.

39. Patel, A.; Dharmarajan, V.; Vought, V. E.; Cosgrove, M. S. On the mechanism of multiple lysine methylation by the human mixed lineage leukemia protein-1 (MLL1) core complex. *J Biol Chem* **2009,** *284*, 24242-24256.

40. Kouskouti, A.; Scheer, E.; Staub, A.; Tora, L.; Talianidis, I. Gene-specific modulation of TAF10 function by SET9-mediated methylation. *Mol Cell* **2004,** *14*, 175-182.

41. Zhang, X.; Cheng, X. Structure of the predominant protein arginine methyltransferase PRMT1 and analysis of its binding to substrate peptides. *Structure* **2003,** *11*, 509-520.

42. Yoo, J.; Medina-Franco, J. L. Inhibitors of DNA methyltransferases: insights from computational studies. *Curr Med Chem* **2012,** *19*, 3475-3487.

43. Friesner, R. A.; Banks, J. L.; Murphy, R. B.; Halgren, T. A.; Klicic, J. J.; Mainz, D. T.; Repasky, M. P.; Knoll, E. H.; Shelley, M.; Perry, J. K.; Shaw, D. E.; Francis, P.; Shenkin, P. S. Glide: A new approach for rapid, accurate docking and scoring. 1. method and assessment of docking accuracy. *J Med Chem* **2004,** *47*, 1739-1749.

44. Xiao, D.; Dasgupta, C.; Chen, M.; Zhang, K.; Buchholz, J.; Xu, Z.; Zhang, L. Inhibition of DNA methylation reverses norepinephrine-induced cardiac hypertrophy in rats. *Cardiovasc Res* **2014,** *101*, 373-382.

Figure legends

Figure 1. In vitro DNMT1 activity assays for compounds. (A) All compounds were tested at 200 μM in the presence of 1% DMSO using the EpiQuik DNA Methyltransferase (DNMT) Activity/Inhibitor Assay Kit (Epigentek). SAH was used as a reference drug (black column). DC_05 (red column) inhibits DNMT1 activity by >60%; (B) Inhibitory activities of DC_05 against DNMT1.

Figure 2. DNMT1 activity assays for the DC_05 analogs against DNMT1. Nineteen DC_05 analogs were tested at 50 μM using a radioactive methylation assay. Eight of the 19 compounds showed more than 50% inhibition of DNMT1 activity (red columns).

Figure 3. SPR assays of the binding between DNMT1 and inhibitors. SPR curves for DNMT1 binding with DC_05 (A) and DC_517 (B) are shown. The concentrations of inhibitors injected over the CM5 chip and were immobilized with DNMT1 protein are indicated. These assays yielded K_D values of 1.09 μM and 0.91 μM for DNMT1 binding with compounds DC_05 and DC_517.

Figure 4. Structures and binding modes of (*R*) and (*S*) enantiomers of DC_05 and DC_517 with DNMT1 (PDB code: 4DA4). (A) The structure of DC_05, the chirality center is depicted as a red star; (B) Activities of DC_05 and its enantiomers against DNMT1; (C) A superimposition of the putative binding modes of (*R*)-DC_05 (yellow) and (*S*)-DC_05 (slate), hydrogen bonds are depicted as dashed red lines; (D) The structure of DC_517 in which the chirality center is depicted as a red star mark; (E) Activities of DC_517 and its enantiomers against DNMT1; and (F) The superimposition of the putative binding modes of (*R*)-DC_517 (orange) and (*S*)-DC_517 (light green). Hydrogen bonds are depicted as dashed red lines.

Figure 5. Putative binding modes of DC_05 and its analogs in the DNMT1 structure (PDB code: 4DA4). (A) The binding modes of DC_05 (yellow) and SAH (green) with DNMT1. (B) The superimposition of the binding modes of DC_05 (yellow), DC_503 (celadon), DC_504 (light blue), DC_508 (orange) and DC_516 (deep pink). The catalytic pocket of DNMT1 is depicted as a white surface; (C) Binding modes of DC_05

(yellow) and DC_501 (cyan); and (D) Binding modes of DC_05 (yellow) and DC_512 (magenta). The DNMT1 structure is depicted as white cartoons and sticks; the hydrophobic region of the SAM pocket is marked as a dashed green circle, and cytosine pocket is marked as a dashed orange circle; the hydrogen bonds are depicted as dashed red lines; chlorines in green and bromines in dark red. For chiral compounds, the chosen binding poses are the corresponding enantiomers that obtained higher docking scores.

Figure 6. The cellular activity of inhibitors. (A) Human colon cell lines were treated with 1.25, 2.5, 5 and 10 μM DC_05, DC_501 and DC_517 for 24, 48, and 72 hours; (B) Human pancreatic adenocarcinoma cell lines were treated with 2.5, 5, 10 and 20 μM DC_05, DC_501 and DC_517 for 24, 48, and 72 hours. (C) Human colon cell lines were treated with 0, 0.75, 1.5 and 3 μM DC_517 for 24 hours and then the cells were assayed for apoptosis by flow cytometry. DC_517 induces apoptotic cell death in HCT116 cells in a dose-dependent manner.

Chart 1. DNMT1 inhibitors

Nucleoside analogs

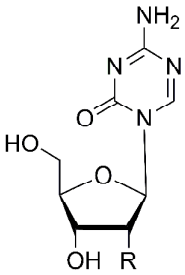

5-Azacytidine (R = OH)
5-Aza-2'-deoxycytidine (R = H)

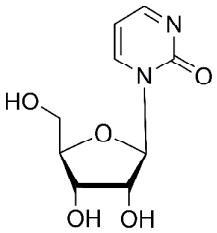

Zebularine

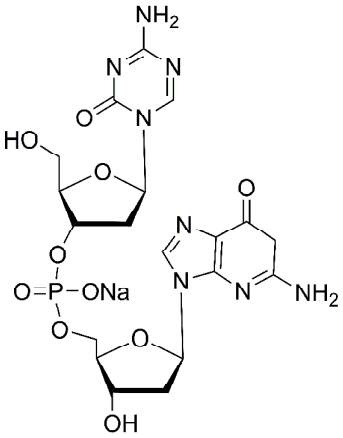

SGI-110

Non-nucleoside analogs

I. Natural compounds

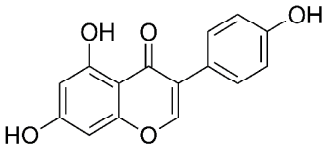

Genistein

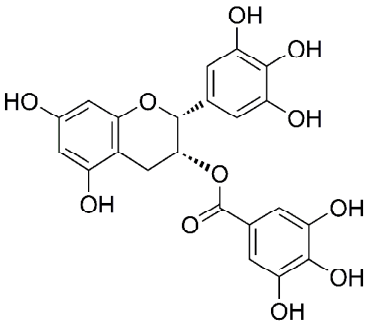

(-)-epigallocatechin-3-O-gallate (EGCG)

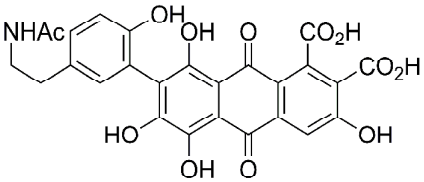

Laccaic acid A

II. Repurposed drugs

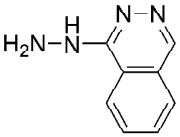

Hydralazine

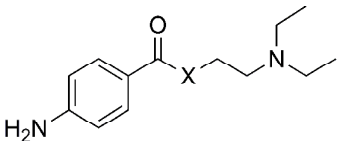

Procainamide (X = NH)
Procaine (X = O)

III. Novel inhibitors

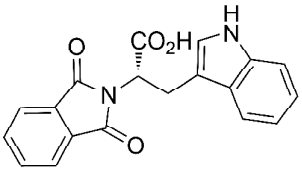

RG108

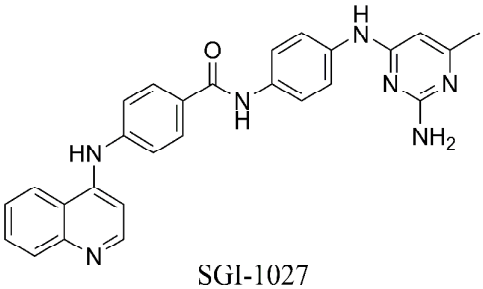

SGI-1027

Table 1. Inhibitory activities of DC_05 against DNMT3A, DNMT3B, G9a, SUV39H1, MLL1, SET7/9 and PRMT1. DC_05 shows a remarkable DNMT1-selectivity (as other methylatransferase IC_{50} ratio)

Protein	IC_{50} (μM)	DNMT1-selectivity
DNMT3A	>200	>19.4
DNMT3B	>200	>19.4
G9a	>150	>14.6
SUV39H1	>150	>14.6
MLL1	>150	>14.6
SET7/9	>150	>14.6
PRMT1	37.1	3.6

Table 2. Biochemical assays results for DC_05 and its analogues against DNMT1 catalytic activity.

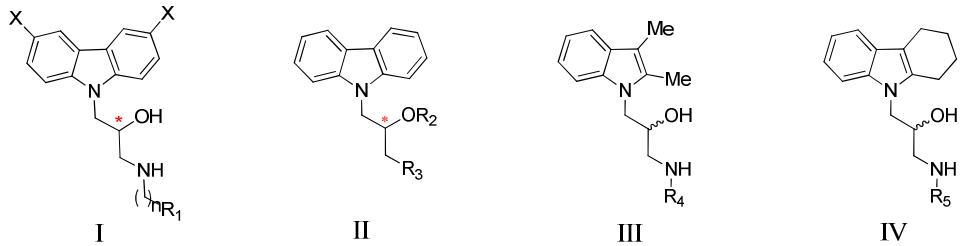

I II III IV

Compound	Scaffold	Substituent	Inh% (50μM)	IC_{50} (μM)	IC_{50} SD(μM)
DC_05	**I**	X = H, R_1 = 1*H*-indol-3-yl, n = 2	--	10.3	0.6
(*R*)-DC_05			--	7.3	2.8
(*S*)-DC_05			--	15.6	6.0
DC_501		X = Cl, R_1 = 1*H*-indol-3-yl, n=2	89.5	2.5	1.3
DC_502		X = H, R_1 = hydroxy, n = 3	42.5	--	--
DC_503		X = H, R_1 = phenyl, n = 2	73.9	20.7	8.7
DC_504		X = H, R_1 = methoxy, n = 2	71.0	29.6	4.6
DC_505		X = H, R_1 = phenoxy, n = 2	29.7	--	--
DC_506		X = H, R_1 = cyclopropyl, n = 0	42.6	--	--
DC_507		X = H, R_1 = tetrahydrofuran-2-yl, n = 1	40.1	--	--
DC_512		X = Br, R_1 = OH, n = 2	99.7	14.1	1.5
DC_509	**II**	R_2 = H, R_3 = 4-methyl-phenylamino	-17.3	--	--
DC_510		R_2 = H, R_3 = 2-ethyl-phenylamino	-14.7	--	--
DC_511		R_2 = H, R_3 =	0.6	--	--

		4-methoxy-phenylamino			
DC_515		R_2 = H, R_3 = *N,N* - dipropyl	5.5	--	--
DC_516		R_2 = H, R_3 = 4-methylpiperidin-1-yl	52.4	84.1	9.0
DC_519		R_2 = H, R_3 = morpholino	-5.0	--	--
DC_508		R_2 = H, R_3 = 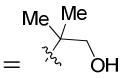	55.7	70.9	9.5
DC_517		R_2 = 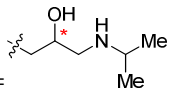 , R_3 = 9-carbazolyl	101.6	1.7	0.6
(*R*)-DC_517			--	2.5	0.6
(*S*)-DC_517			--	1.8	0.3
DC_513	**III**	R_4 = methyl	1.1	--	--
DC_518		R_4 = cyclohexyl	2.4	--	--
DC_514	**IV**	R_5 = benzyl	62.9	80.9	19.4

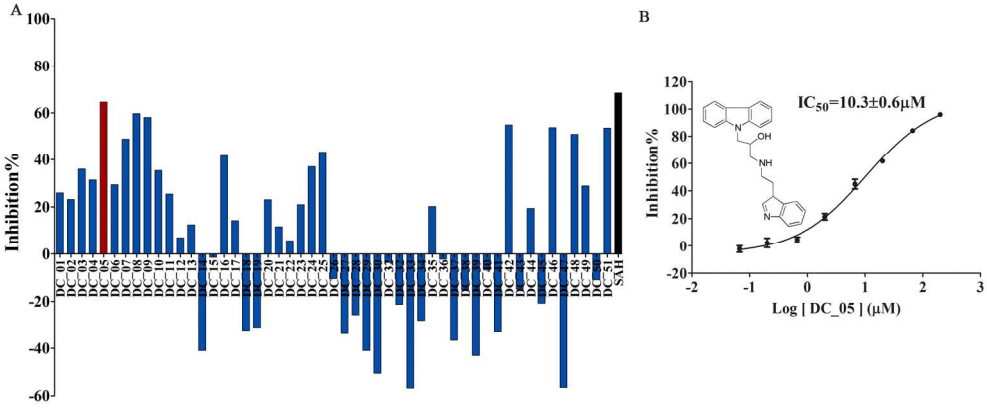

Figure 1. In vitro DNMT1 activity assays for compounds. (A) All compounds were tested at 200 μM in the presence of 1% DMSO using the EpiQuik DNA Methyltransferase (DNMT) Activity/Inhibitor Assay Kit (Epigentek). SAH was used as a reference drug (black column). DC_05 (red column) inhibits DNMT1 activity by >60%; (B) Inhibitory activities of DC_05 against DNMT1.
175x77mm (300 x 300 DPI)

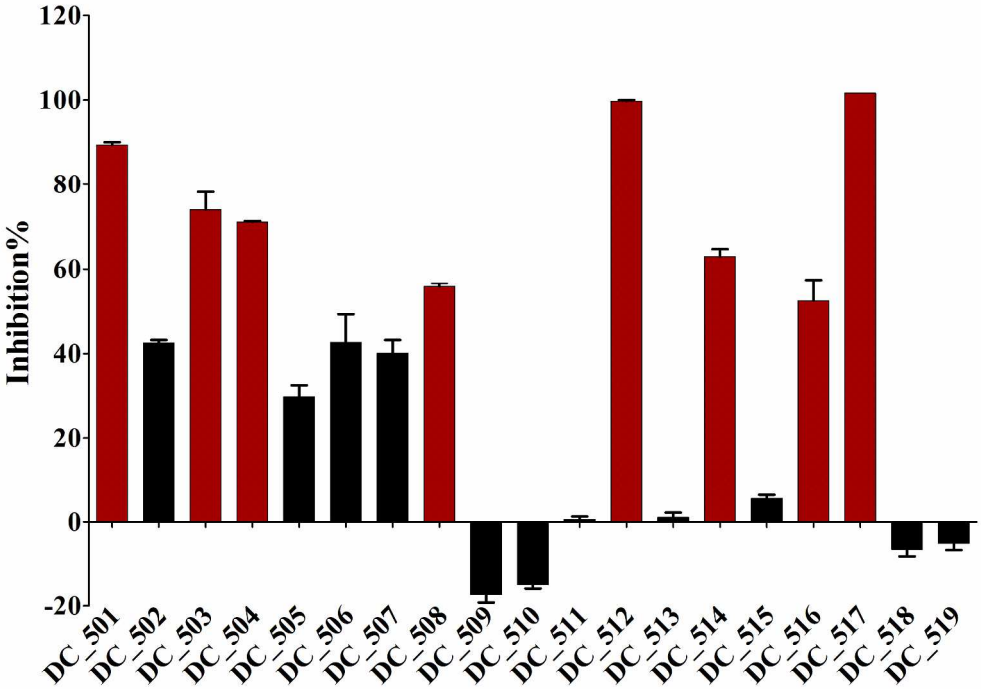

Figure 2. DNMT1 activity assays for the DC_05 analogs against DNMT1. Nineteen DC_05 analogs were tested at 50 μM using a radioactive methylation assay. Eight of the 19 compounds showed more than 50% inhibition of DNMT1 activity (red columns)
281x203mm (300 x 300 DPI)

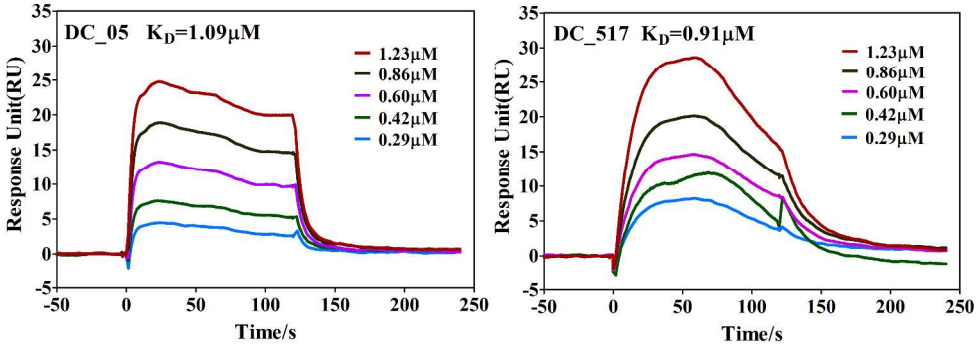

Figure 3. SPR assays of the binding between DNMT1 and inhibitors. SPR curves for DNMT1 binding with DC_05 (A) and DC_517 (B) are shown. The concentrations of inhibitors injected over the CM5 chip and were immobilized with DNMT1 protein are indicated. These assays yielded KD values of 1.09 μM and 0.91 μM for DNMT1 binding with compounds DC_05 and DC_517.
360x145mm (300 x 300 DPI)

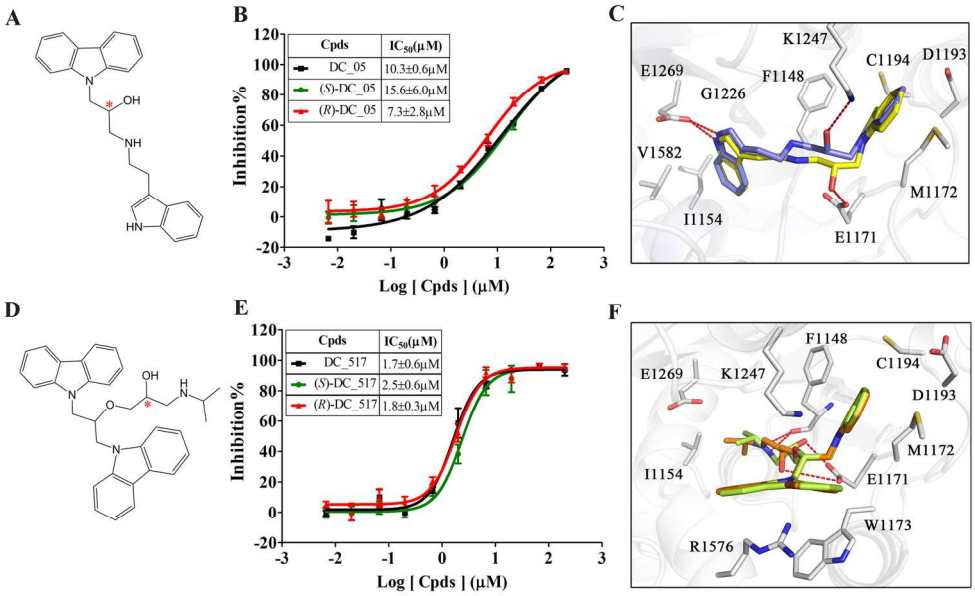

Figure 4. Structures and binding modes of (R) and (S) enantiomers of DC_05 and DC_517 with DNMT1 (PDB code: 4DA4). (A) The structure of DC_05, the chirality center is depicted as a red star; (B) Activities of DC_05 and its enantiomers against DNMT1; (C) A superimposition of the putative binding modes of (R)-DC_05 (yellow) and (S)-DC_05 (slate), hydrogen bonds are depicted as dashed red lines; (D) The structure of DC_517 in which the chirality center is depicted as a red star mark; (E) Activities of DC_517 and its enantiomers against DNMT1; and (F) The superimposition of the putative binding modes of (R)-DC_517 (orange) and (S)-DC_517 (light green). Hydrogen bonds are depicted as dashed red lines.
175x111mm (300 x 300 DPI)

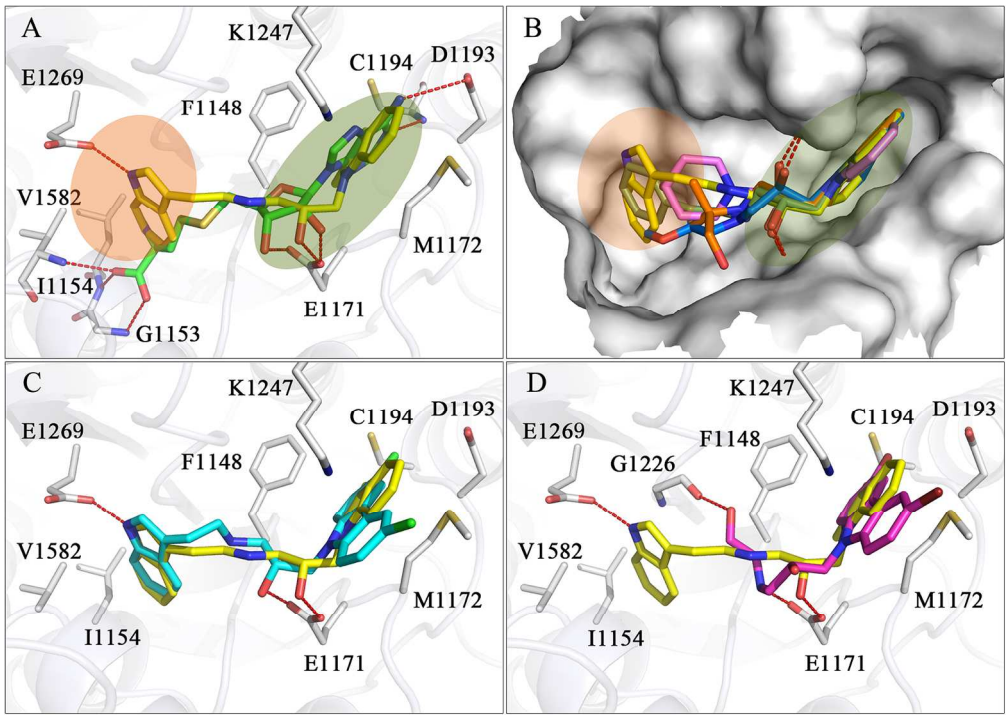

Figure 5. Putative binding modes of DC_05 and its analogs in the DNMT1 structure (PDB code: 4DA4). (A) The binding modes of DC_05 (yellow) and SAH (green) with DNMT1. (B) The superimposition of the binding modes of DC_05 (yellow), DC_503 (celadon), DC_504 (light blue), DC_508 (orange) and DC_516 (deep pink). The catalytic pocket of DNMT1 is depicted as a white surface; (C) Binding modes of DC_05 (yellow) and DC_501 (cyan); and (D) Binding modes of DC_05 (yellow) and DC_512 (magenta). The DNMT1 structure is depicted as white cartoons and sticks; the hydrophobic region of the SAM pocket is marked as a dashed green circle, and cytosine pocket is marked as a dashed orange circle; the hydrogen bonds are depicted as dashed red lines; oxygen atoms in ligands are shown in red, sulfur in yellow, nitrogens in blue, chlorines in green and bromines in dark red. For chiral compounds, the chosen binding poses are the corresponding enantiomers that obtained higher docking scores.
175x124mm (300 x 300 DPI)

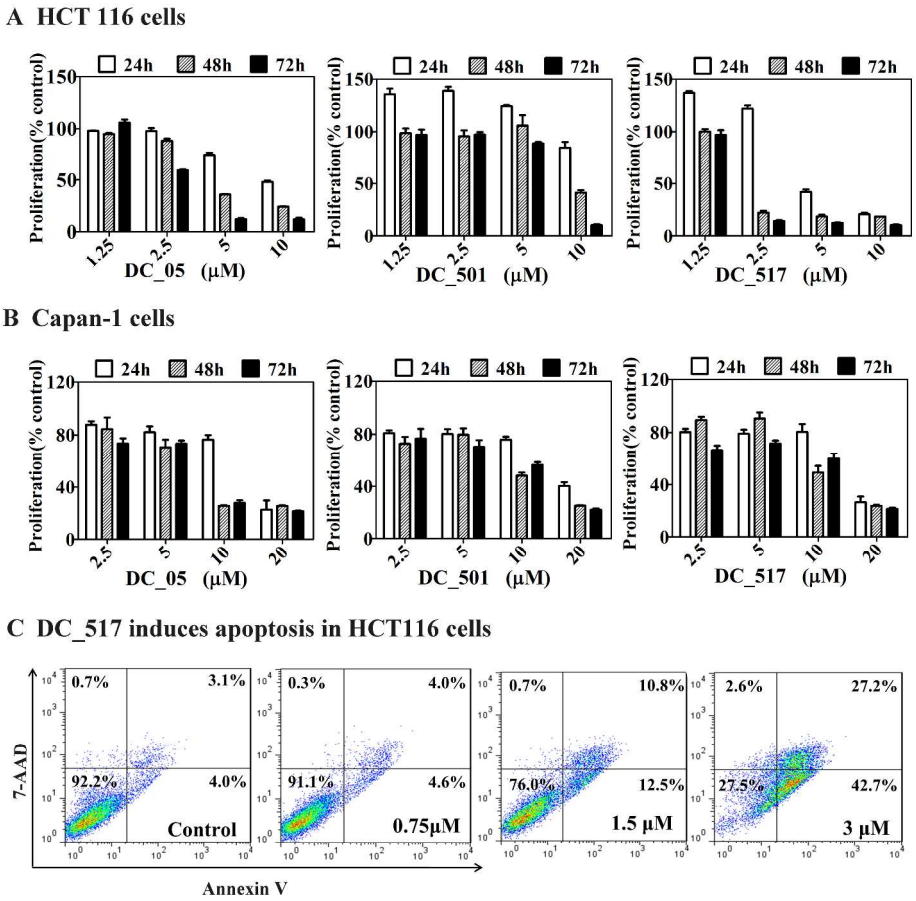

Figure 6. The cellular activity of inhibitors. (A) Human colon cell lines were treated with 1.25, 2.5, 5 and 10 μM DC_05, DC_501 and DC_517 for 24, 48, and 72 hours; (B) Human pancreatic adenocarcinoma cell lines were treated with 2.5, 5, 10 and 20 μM DC_05, DC_501 and DC_517 for 24, 48, and 72 hours. (C) Human colon cell lines were treated with 0, 0.75, 1.5 and 3 μM DC_517 for 24 hours and then the cells were assayed for apoptosis by flow cytometry. DC_517 induces apoptotic cell death in HCT116 cells in a dose-dependent manner.
340x330mm (300 x 300 DPI)

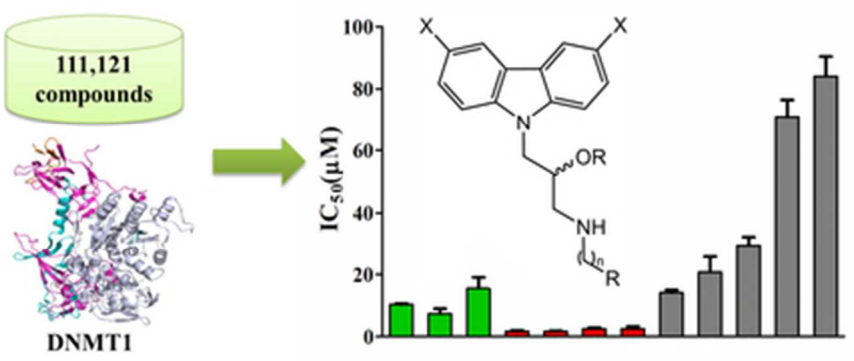

Table of Contents graphic
36x15mm (300 x 300 DPI)